Growth of Ordered Graphene Ribbons by Sublimation Epitaxy

Shuxian Cai [1,2], **Xingfang Liu** [3,*], **Xin Zheng** [2] **and Zhonghua Liu** [1,2,*]

[1] National Research Center of Engineering Technology for Utilization of Botanical Functional Ingredients, Hunan Agricultural University, Changsha 410128, China; caishuxian@hunau.edu.cn

[2] Key Laboratory of Ministry of Education for Tea Science, Hunan Agricultural University, Changsha 410128, China; zhengxin@stu.hunau.edu.cn

[3] Key Laboratory of Semiconductor Materials Science, Institute of Semiconductors, Chinese Academy of Sciences, Beijing 100083, China

[*] Correspondence: liuxf@mail.semi.ac.cn (X.L.); larkin-liu@163.com (Z.L.); Tel.: +86-10-8230-4101 (X.L.); +86-731-8463-5304 (Z.L.)

Abstract: Ordered graphene ribbons were grown on the surface of $4°$ off-axis 4H-SiC wafers by sublimation epitaxy, and characterized by using scanning electron microscopy (SEM), atomic force microscopy (AFM) and micro-Raman spectroscopy (μ-Raman). SEM showed that there were gray and dark ribbons on the substrate surface, and AFM further revealed that these ordered graphene ribbons had clear stepped morphologies due to surface step-bunching. It was shown by μ-Raman that the numbers of graphene layers of these two types of regions were different. The gray region was composed of mono- or bilayer ordered graphene ribbon, while the dark region was of tri- or few-layer ribbon. Meanwhile, ribbons were all homogeneous and had a width up to 40 μm and a length up to 1000 μm, without micro defects such as grain boundaries, ridges, or mono- and few-layer graphene mixtures. The results of this study are useful for optimized growth of high-quality graphene film on silicon carbide crystal.

Keywords: graphene; ribbon; 4H-SiC; sublimation; epitaxy; Raman

1. Introduction

Due to its unique properties, such as the unusual half-integer quantum Hall effect [1,2] and mass-less Dirac fermion behavior [3,4], graphene has many potential applications in the fields of novel physics, chemistry, optics, and mechanics [5,6], and as realistic technology transfer in the fields of membrane technology [7], energy [8], photodetection [9], and plasmonics [10]. Since the successful preparation of the first stable graphene flake at room temperature by peeling highly oriented pyrolytic graphite (HOPG) [11], people have developed many methods to prepare graphene, including monolayer [12,13], bilayer [14,15], and few-layer graphene [16,17], in the form of powder [18], flake [19], and film [20]. Although intrinsic monolayer graphene is a semimetal without a bandgap, we can open a specific bandgap by patterning graphene into nano-ribbons or coupling graphene with certain substrates [21,22]; bilayer graphene can be operated to have a high on/off ratio, and a bandgap up to hundreds of millielectronvolts controlled by an electronic field, which paves the way for its applications in high performance electronics [23].

In order to increase output and be compatible with microelectronics processes, large scale graphene films are needed. Today, growth of graphene on metal foils such as Cu foils by using chemical vapor deposition (CVD) has been proven to be a good preparation method, and has been adopted throughout the world [24–27]. Since large volume metal foils are commercially available,

theoretically people can grow arbitrarily large areas of graphene films, and indeed roll-to-roll growth of large scale graphene films on Cu foils has been demonstrated [28]. Meanwhile, there are drawbacks of this preparation of graphene films. For example, since the Cu foils are of polycrystalline structure, graphene grown on Cu foils is also of polycrystalline structure, which greatly degrades the performance of the graphene. The good news is that it is feasible to develop single crystal graphene with areas up to square centimeters on Cu foil [29].

Besides, growth of large scale graphene films on single crystal silicon carbide wafers such as 4H-SiC has been proven to be a great potential method [30–34]. 4H-SiC Wafers are commercially available with a diameter up to 6 inches, and it is convenient to fabricate graphene devices on 4H-SiC with compatible processes of silicon. As for graphene preparation, 4H-SiC has several intrinsic advantages. First, 4H-SiC is made of silicon and carbon, which makes it possible to form graphene on the surface of the wafer by sublimating the silicon element. This is realizable since the vapor pressure of Si is greater than that of carbon, and indeed graphene has been prepared by this method [35]. Second, large scale semi-insulating 4H-SiC wafers (SI-SiC) are commercially available and can be used for graphene preparation. This makes graphene devices able to be fabricated directly on SI-SiC wafers without a transfer of graphene to the foreign substrate, which overcomes the drawback of graphene grown on metal foil [36,37]. Third, and we think the most important point, fine graphene with elegant structures can be prepared on mis-cut 4H-SiC wafers through direct growth without complicated processes. There are nano-steps on the surface of a mis-cut 4H-SiC wafer (typically 4° off-axis), which act as templates for the preparation of exquisite graphene, such as nano-ribbons [38]. In the surface of 4° off-axis 4H-SiC wafers, the height of the step is several nanometers, and the width of the terrace is several tens of nanometers. Nano-ribbons formed on the steps and terraces are demonstrated [39], with similar lateral sizes to the templates, and monolayer and few-layer (2–5 layers) graphene is also prepared on these templates. In addition, the lateral sizes of the nano-steps of 4° off-axis 4H-SiC wafer can be enlarged by heat treatment or homoepitaxial growth [40,41] through step-bunching [42–44]. In doing so, it is possible to obtain as-grown graphene ribbons with a lateral size up to several tens of micrometers.

In this paper, we investigated the process of growth of high-quality graphene ribbons. We used 4° off-axis 4H-SiC wafers as a substrate, and we grew ordered and homogeneous graphene ribbons across the whole surface of the wafer, with a width up to 40 μm and a length up to 1000 μm. It is worth noting that the ordered ribbons grown along the templates did not have any micro defects such as grain boundaries, ridges, or mono- and few-layer graphene mixtures, compared to graphene grown on on-axis 4H-SiC wafer whose surface is nearly step-free [45,46]. Our results shed light on the growth of high-quality graphene film on silicon carbide crystal.

2. Materials and Methods

2.1. Materials

N-type 4° off-axis 4H-SiC(0001) Si-face wafers were used as the target and source wafers. Wafers were cleaned in (1) boiling H_2SO_4, and hot solutions of (2) $NH_3 + H_2O_2 + H_2O$ (1:1:5 vol%) and (3) $HCl + H_2O_2 + H_2O$ (1:1:6 vol%) in sequence. After each cleaning process, wafers were rinsed in distilled water. Finally, wafers were blown dry with hot nitrogen gas and immediately loaded into the growth chamber.

2.2. Apparatus

The graphene growth process was conducted in a home-made sublimation epitaxy reactor. The reactor has a vertical hot-wall chamber. Figure 1a shows the schematic illustration of the chamber. Its main parts include radio frequency (RF) coils for heating graphite parts, a gas inlet and gas outlet for gas injecting and exhaustion, a pyrometer for temperature monitoring, and a graphite susceptor for holding the wafer container. Figure 1b shows the wafer container with wafers loaded. The graphite

container can be heated by RF coils to a temperature of about 1850 °C. The source wafer was placed on the bottom of the container, and the target wafer was hung at the top of the container. They can be heated to 1800 °C and 1750 °C, respectively, monitored by the pyrometer. Since the target wafer did not touch graphite parts (except for wafer edge) and there was a 5 mm spacer between the target wafer and the source wafer, the temperature of the target wafer was lower than that of the source wafer by about 50 °C.

2.3. Methods

The temperature gradient between the source wafer and the target wafer was used to perform the sublimation process. Molecules containing Si-C components sublimate from source wafer on the bottom of the container, and condense and crystallize on the surface of the target wafer at the top of the container.
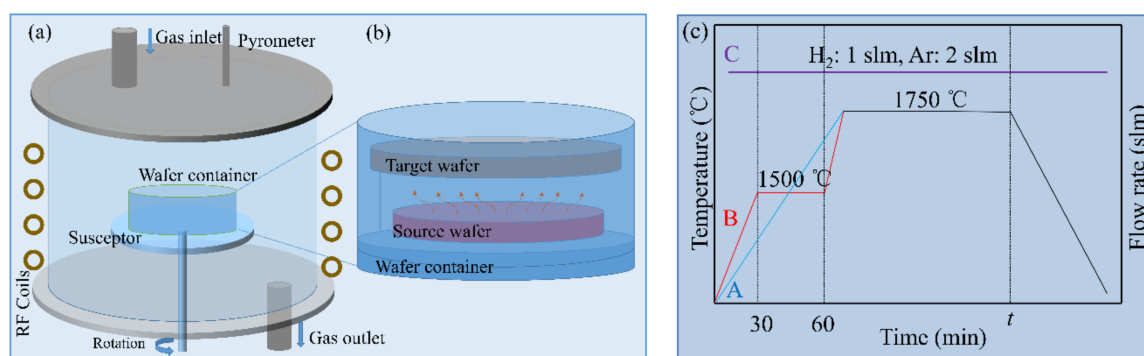

Figure 1. Schematic illustration of (**a**) sublimation epitaxy chamber and (**b**) wafer container with source wafer and target wafer loaded; (**c**) growth process.

Figure 1c shows the growth process. Three protocols were used in our experiments: A) Target wafer was directly heated to 1750 °C under high vacuum; B) Target wafer was subjected to a heat treatment at 1500 °C for 30 min, and then heated to 1750 °C for growth under high vacuum; C) based on B, a gas mixture of 1 slm H_2 and 2 slm Ar with a pressure of 5 kPa or 10 kPa was used. The growth time (*t*) varied from 30 min to 60 min. For convenience, samples obtained from protocols A, B, and C are labelled as Wafer A, Wafer B, and Wafer C, respectively. Wafer C can be labelled as Wafer C1 and C2, due to the used pressure of 5 kPa and 10 kPa, respectively.

After growth, the samples were examined by means of scanning electron microscope (SEM) (2011, Hitachi Inc., Tokyo, Japan), optical microscope (OM) (2009, Olympus Inc., Tokyo, Japan), atomic force microscope (AFM) (2007, Vecco Inc., Plainview, NY, USA) and Raman spectrometer (μ-Raman) (2008, Horiba Jobin Yvon Inc., Montpellier, France). The Raman has an Ar laser operated at 532 nm, and the focused laser spot was of about 1 μm in diameter.

3. Results and Discussion

3.1. Effect of Heat Treatment

Figure 2 shows SEM images of the surfaces of Wafer A and Wafer B. The dark domains in the images are graphene regions. It can be seen from Figure 2a that there were graphene flakes grown on the surface of Wafer A. The flakes distributed randomly on the surface, and most of them took on a strip profile. The lateral size of a typical largest flake can be measured to be 42 μm × 14 μm (Figure S1a). Figure 2b is a magnified view of Figure 2a, from which more details of the relationship between the graphene flakes and the surface of 4H-SiC can be observed. There are irregular terrace-steps on the surface, and the flakes are on top of the terraces. Some large graphene strips cover several terrace-steps continuously. The above results indicate that graphene can be grown on the surface of target 4H-SiC wafer by sublimation epitaxy through protocol A. However, the obtained graphene is in flakelets,

which means we cannot grow graphene ribbon through protocol A. On the other hand, the result also implies that the terrace-step structures may be used to guide the growth of graphene ribbon, since the graphene flakes will grow along with the terraces. If regular and long terraces could be prepared on the wafer surface, it would favor the growth of ordered graphene ribbons.

It has been reported that terrace-step structures will form on the surface of off-axis 4H-SiC wafer after a heat treatment [47,48]. In protocol B, we performed a 30-min heat treatment at 1500 °C for 30 min before sublimation growth of graphene. It can be seen from Figure 2c,d that in general, the graphene strips distributed in parallel on the surface, and the shape of graphene changed from flake to strip, compared in Figure 2, with a typical lateral size of about 100 μm × 10 μm (Figure 2d). We observed that terrace-step structures indeed appeared on the surface of target wafer after a heat treatment in protocol B (Figure S1b), and the structures still survived on the surface after the sublimation growth of graphene (Figure 2). This indicates that heat treatment is useful for the growth of ordered graphene strips. However, in protocol B we only obtained ordered strips, not ordered ribbons. The duration of the sublimation growth for Figure 2d was double that of Figure 2c, about 60 min. Although graphene strips became wider and longer, they still did not merge into ordered ribbons.
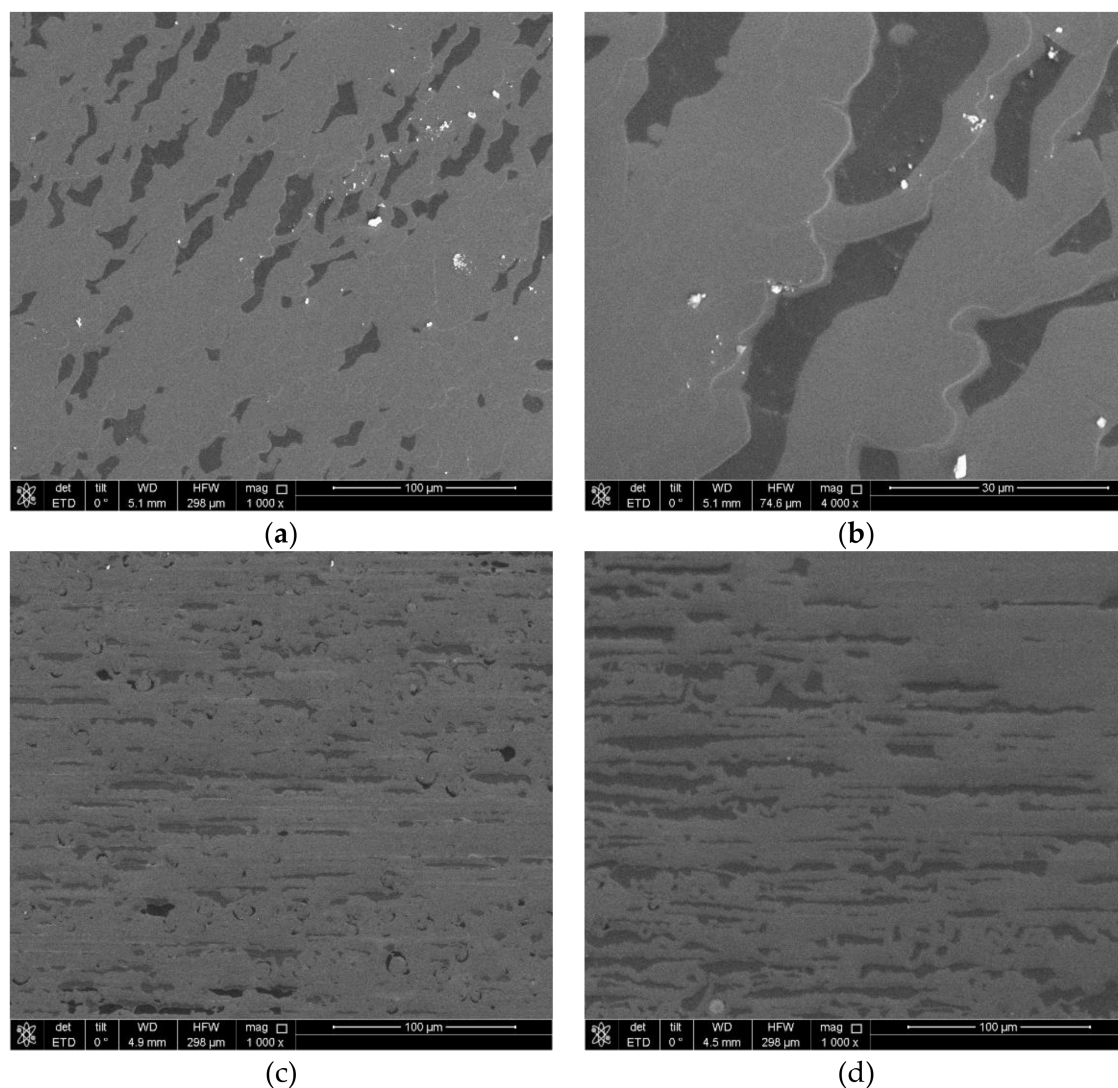

Figure 2. Scanning electron microscope (SEM) images of the surfaces of target wafers: (**a**) surface of Wafer A; (**b**) magnified view of (**a**); (**c,d**) surface of Wafer B.

3.2. Role of Gas Mixture

In protocol C, we used a gas mixture of H_2 and Ar during the whole process. Figure 3 shows SEM images and an optical image of the surface morphologies of Wafer C. The morphologies are quite different compared with those of Figure 2. Here, the obtained graphene is in ordered graphene ribbons. In Figure 3a, the ribbons are long and straight, covering most of the areas of the surface, with less space bared for raw surface (i.e., the gray regions), and most ribbons almost merge together in the width direction. However, in a magnified view of the graphene ribbons (Figure 3b), the ribbons are not totally free of raw surface of 4H-SiC substrate. There are meshed residues of raw surface existing in the ribbons. This indicates that the quality of the obtained graphene ribbons should be further improved.
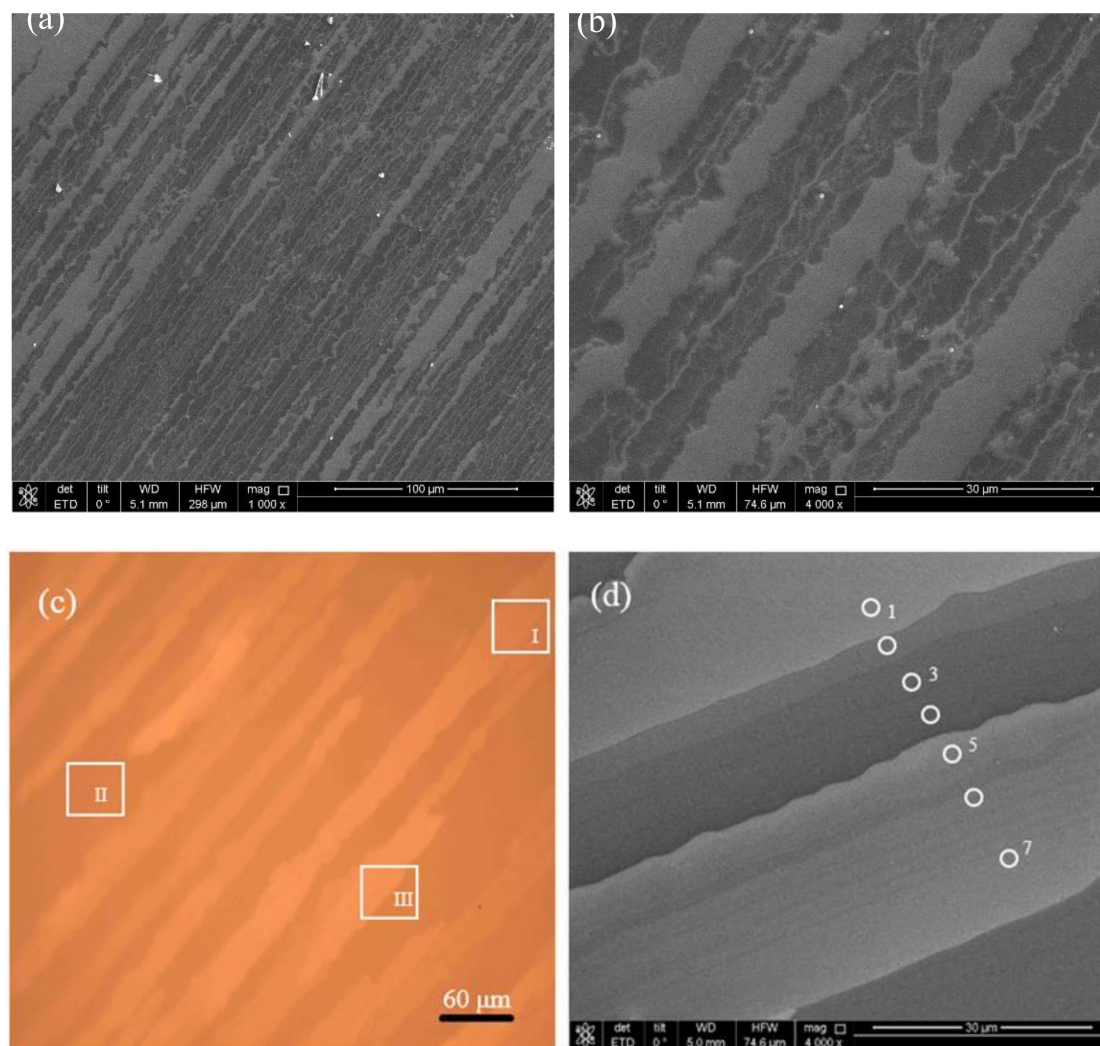

Figure 3. Surface morphology of Wafer C: (**a**,**b**) SEM images of surface of Wafer C1; (**c**) optical image and (**d**) SEM image of Wafer C2.

It can also be observed from Figure 3b that the graphene ribbons (dark regions) and the raw surface (gray regions) were neatly parallel to each other. This gave us a hint that protocol C was a suitable scheme for preparation of ordered graphene ribbons, and what needed to be done was to optimize the process conditions. To this end, we changed the growth pressure. We grew graphene in high vacuum conditions in protocol A and protocol B, and under a low pressure of 5 kPa in protocol C1. The results shown in Figures 2 and 3,b reveal that a proper growth pressure will be good for graphene preparation. In protocol C2, we set the growth pressure to be 10 kPa. The surface morphologies of Wafer C2 are shown in Figure 3c,d. It can be seen that ordered graphene ribbons were obtained on the

surface of Wafer C2. Note that the gray ribbons and the dark ones of Wafer C2 were all of graphene, identified by Raman measurements (see Subsection 3.3). The gray and the dark ribbons occupied the surface evenly, in a side-by-side pattern, with a length up to 1000 μm, which is totally different to the results of Wafer A and Wafer B. The ribbons were of whole graphene, without any residue of raw surface, which was far better than those of Wafer C1. This indicates that ordered graphene ribbons can be obtained through protocol C2.

Next, we examined the finer structure of the graphene ribbons by using AFM. We chose three square regions on Wafer C2: I. Gray ribbon on the surface; II. Dark ribbon; III. Cross region between the gray and the dark ribbon. The white open squares in Figure 3c show these regions, and the AFM images are shown in Figure 4a–c. It obviously shows that there were terrace-step structures in each region, and that the structures were made up of many small steps and one to several large steps. Figure 4a has the highest density of small steps, and Figure 4b has the second highest. This indicates that the terraces on the surface of Wafer C2 became wider after graphene growth, compared with the terraces on the original surface of the 4° off-axis 4H-SiC(0001) wafer. Figure 4d shows line section analyses of the AFM images, from which we can see the dimensions of each terrace and each step for the three regions. The scale of the small step for three regions was almost the same, while the large step varied, and was at its largest in region III. The largest step means that there was a huge step between a gray graphene ribbon and a dark one on the surface.
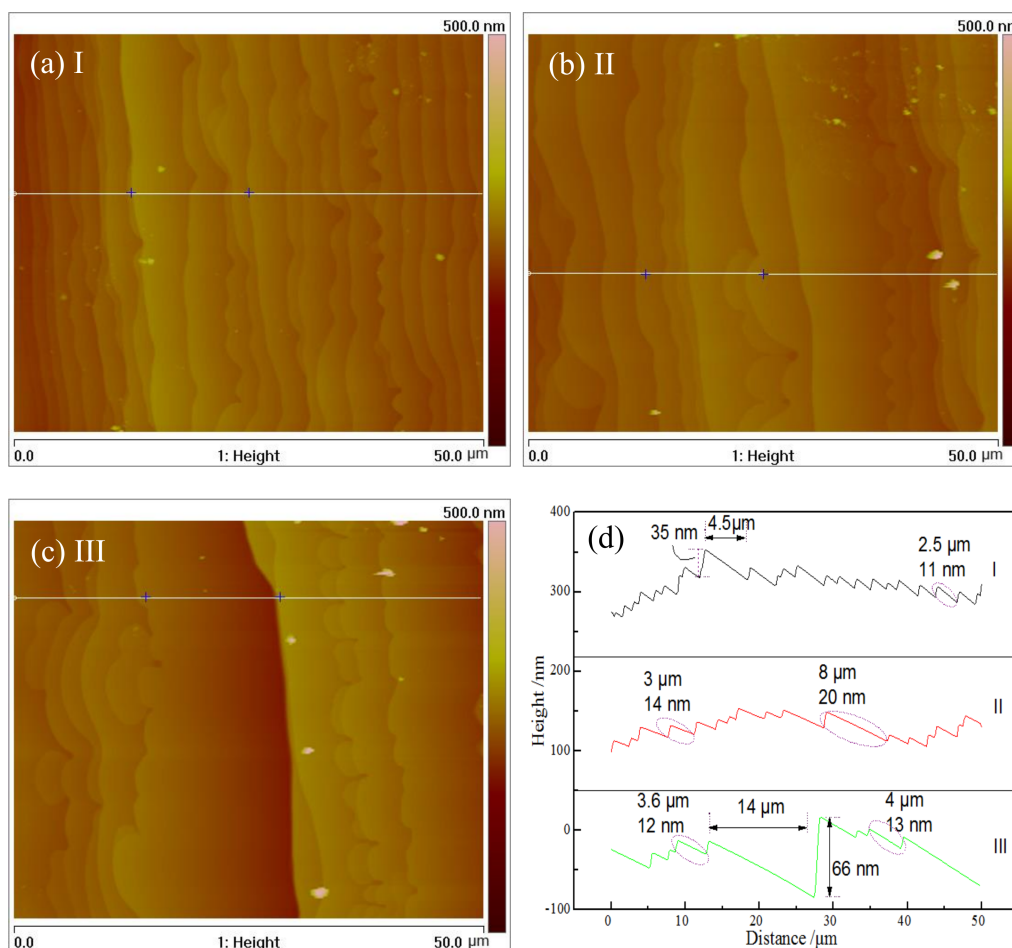

Figure 4. Atomic force microscope (AFM) analysis of surface of Wafer C2: (**a**) region I; (**b**) region II; (**c**) region III marked in Figure 3c; (**d**) section analysis for corresponding regions in (**a**–**c**).

3.3. Graphene Characterization

Raman measurements were used to identify and characterize graphene grown on the surface of Wafer C2. Micro-Raman spectroscopy is a powerful but non-invasive technique for graphene characterization [49]. Figure 5 shows Raman spectra in range of 1200–2800 cm^{-1}, collected from the points of the surface of Wafer C2 marked in Figure 3d with white open circles. In this wavelength range, the characteristic peaks of graphene, namely D peak, G peak, and 2D peak, will appear [50]. The D peak, located at about 1350 cm^{-1}, is the characteristic peak for graphene defects such as grain boundaries and edges. The G peak at about 1580 cm^{-1} originates from in-plane vibration of sp^2 carbon atoms, and the 2D peak at about 2700 cm^{-1}, which is associated with the phonon resonance near the *K* points in the Brillouin zone [51], is the fingerprint peak of graphene. It should be noted that the second-order Raman spectrum of 4H-SiC is in the range of 1400–1800 cm^{-1} [52], and it will disturb the identification of D peak and G peak of graphene. It is better to subtract the 4H-SiC Raman signals at this wavelength range from graphene Raman spectra.
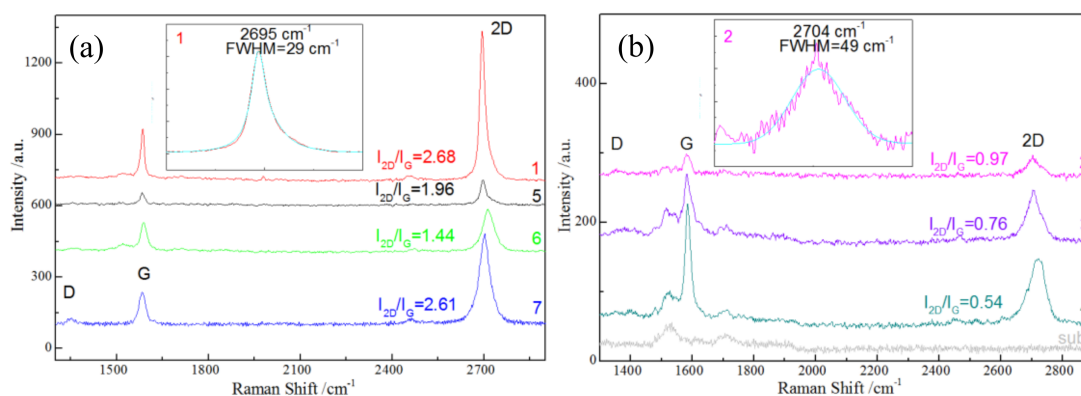

Figure 5. Raman spectra collected from points of surface of Wafer C2, marked in Figure 3d.

Although we did not find graphene signals on the gray regions of the surfaces of Wafer A (and Wafer B), we found clear graphene signals on the counterpart of Wafer C2 (Figure 5a). In the Raman spectrum of point 1 (red spectrum in Figure 5a), for example, the D peak does not appear, which indicates that the graphene ribbon was defect-free. The 2D peak is symmetrical, and can be fitted perfectly by a Lorentz peak (insert in Figure 5a). The number of graphene layers, and the crystalline quality, can be characterized by means of the ratio of the intensity of the 2D peak to the intensity of the G peak (I_{2D}/I_G), combined with the full width at half maxima (FWHM) of the 2D peak. Graphene is monolayer when $I_{2D}/I_G > 2$ and FWHM < 33 cm^{-1} [27], and is bilayer when $1 < I_{2D}/I_G < 2$ [23]. When $I_{2D}/I_G < 1$, the number of layers can be 3–5, which can be further identified by FWHM of the 2D peak and the contrast of the SEM image. In Figures 5a and 3d, it is revealed that the gray graphene ribbon was monolayer or bilayer, and its width varied from several micrometers to several tens of micrometers. Since the ribbon grew on top of the terrace and the terraces were parallel to each other, the ribbons were neat and ordered.

Figure 5b shows Raman spectra of the dark region of the surface of Wafer C2. The I_{2D}/I_G of each spectrum is less than 1, which means that the dark region was multiple-layer. Judging from Figures 3 and 5, we can further identify the number of graphene layers of the dark region. Since point 5 and point 6 of the gray region (the black and the green spectrum in Figure 5a) are bilayer, and the contrast of the SEM image in point 2 (the pink spectrum in Figure 5b) is darker than in point 5, combined with judgments of I_{2D}/I_G (close to 1) and FWHM of 2D peak (49 cm^{-1}), it is reasonable to deduce that point 2 of the dark region was trilayer. For the same reasons, point 3 and point 4 of the dark region may have been 4-layer and 5-layer, respectively (the Lorentz fitting and the FWHM of 2D peak can be found in Figure S4). Again, the trilayer or multiple-layer graphene ribbons of the dark region were neat and ordered, just as the ribbons of the gray region were.

Finally, we give an explanation of the reason why the growth conditions for Wafer C2 were suitable to synthesize neat and ordered graphene ribbons. There are evenly-distributed nano-steps on the surface of 4° off-axis 4H-SiC(0001) Si-face wafers. After the wafers were subjected to a high-temperature heat treatment, the nano-steps kept in order and the terraces of the nano-steps became wider, due to step kinetics or thermodynamic faceting of the inherent characteristics of 4H-SiC [42,43]. Then, sublimation epitaxy of 4H-SiC via step-control mode [43], together with graphene growth, started at a proper growth condition. Among the parameters of the growth condition, the growth pressure played an important role on the terrace-steps on the wafer surface, since it affected the carbon-to-silicon atomic ratio (C/Si ratio) in the process of sublimation [53,54]. An excessive C/Si ratio will cause the appearance of giant steps with wider terraces [42]. This is the reason of why huge steps appear in Figure 4c. On the other hand, during the 4H-SiC homoepitaxy, graphene grew on the 4H-SiC epitaxial layers by sublimation of the Si component at high temperature. The topmost Si-C bilayers of 4H-SiC on the terraces tended to form a monolayer of graphene. Thereafter, as the growth progressed, new Si-C bilayers covered parts of these terraces and converted to another monolayer of graphene on top of the older ones, which formed bilayer of graphene. Repeating this growth-convert process, trilayer and multiple-layer of graphenes also formed on the terraces. Since the ribboned terraces were neat and ordered, so was the graphene. In short, the growth conditions, i.e., 4° off-axis 4H-SiC(0001) Si-face wafer, high-temperature heat treatment, and a growth pressure, were key parameters in synthesis of neat and ordered graphene ribbons.

4. Conclusions

In summary, ordered graphene ribbons were grown on 4° off-axis 4H-SiC wafers, with growth conditions of a heat treatment at 1500 °C for 30 min, and sublimation epitaxy at 1750 °C under a pressure of 10 kPa in a gas mixture of 1 slm H_2 and 2 slm Ar, and the feature sizes of the as-grown ribbons were up to 40 μm in width and 1000 μm in length. These ribbons were homogeneous and defect-free, without micro-defects such as grain boundaries, ridges, or mono- and few-layer graphene mixtures. This is attributed to the enlarged macro-steps which acted as growth templates during sublimation epitaxy.

Supplementary Materials: The following are available online at http://www.mdpi.com/2073-4352/8/12/449/s1. Figure S1: SEM images of (**a**) surface of Wafer A; (**b**) surface of target wafer after a heat treatment. Figure S2: SEM images of surface of (**a**) Wafer C1 and (**b**) Wafer C2; optical images of surface of (**c**,**d**) Wafer C2. Figure S3: A 5 μm × 5 μm AFM analysis of dark ribbon on the surface of Wafer C2. Figure S4: Lorentz fitting and the FWHM of 2D peak of Raman spectrum of (**a**) point 3 and (**b**) point 3.

Author Contributions: Conceptualization, X.L.; methodology, S.C.; validation, Z.L.; formal analysis, S.C. and X.Z.; investigation, S.C. and X.Z.; resources, X.L.; data curation, X.L.; writing—original draft preparation, S.C.; writing—review and editing, X.L.; supervision, X.L.; project administration, Z.L.; funding acquisition, S.C. and X.L.

Conflicts of Interest: The authors declare no conflict of interest.

References

1. Zhang, Y.B.; Tan, Y.W.; Stormer, H.L.; Kim, P. Experimental observation of the quantum Hall effect and Berry's phase in graphene. *Nature* **2005**, *438*, 201–204. [CrossRef] [PubMed]
2. Ding, K.-H.; Lim, L.-K.; Su, G.; Weng, Z.-Y. Quantum Hall effect in ac driven graphene: From the half-integer to the integer case. *Phys. Rev. B* **2018**, *97*, 035123. [CrossRef]
3. Novoselov, K.S.; Geim, A.K.; Morozov, S.V.; Jiang, D.; Katsnelson, M.I.; Grigorieva, I.V.; Dubonos, S.V.; Firsov, A.A. Two-dimensional gas of massless Dirac fermions in graphene. *Nature* **2005**, *438*, 197–200. [CrossRef] [PubMed]
4. Luo, C.W.; Tseng, P.S.; Chen, H.J.; Wu, K.H.; Li, L.J. Dirac fermion relaxation and energy loss rate near the Fermi surface in monolayer and multilayer graphene. *Nanoscale* **2014**, *6*, 8575–8578. [CrossRef] [PubMed]
5. Geim, A.K.; Novoselov, K.S. The rise of graphene. *Nat. Mat.* **2007**, *6*, 183–191. [CrossRef] [PubMed]

6. Ren, S.; Rong, P.; Yu, Q. Preparations, properties and applications of graphene in functional devices: A concise review. *Ceram. Int.* **2018**, *44*, 11940–11955. [CrossRef]

7. Zhou, K.G.; Vasu, K.S.; Cherian, C.T.; Neek-Amal, M.; Zhang, J.C.; Ghorbanfekr-Kalashami, H.; Huang, K.; Marshall, O.P.; Kravets, V.G.; Abraham, J.; et al. Electrically controlled water permeation through graphene oxide membranes. *Nature* **2018**, *559*, 236–240. [CrossRef] [PubMed]

8. Politano, A.; Cattelan, M.; Boukhvalov, D.W.; Campi, D.; Cupolillo, A.; Agnoli, S.; Apostol, N.G.; Lacovig, P.; Lizzit, S.; Farias, D.; et al. Unveiling the Mechanisms Leading to H-2 Production Promoted by Water Decomposition on Epitaxial Graphene at Room Temperature. *ACS Nano* **2016**, *10*, 4543–4549. [CrossRef] [PubMed]

9. Koppens, F.H.L.; Mueller, T.; Avouris, P.; Ferrari, A.C.; Vitiello, M.S.; Polini, M. Photodetectors based on graphene, other two-dimensional materials and hybrid systems. *Nat. Nanotechnol.* **2014**, *9*, 780–793. [CrossRef] [PubMed]

10. Politano, A.; Chiarello, G. Plasmon modes in graphene: Status and prospect. *Nanoscale* **2014**, *6*, 10927–10940. [CrossRef] [PubMed]

11. Novoselov, K.S.; Geim, A.K.; Morozov, S.V.; Jiang, D.; Zhang, Y.; Dubonos, S.V.; Grigorieva, I.V.; Firsov, A.A. Electric field effect in atomically thin carbon films. *Science* **2004**, *306*, 666–669. [CrossRef] [PubMed]

12. Bointon, T.H.; Barnes, M.D.; Russo, S.; Craciun, M.F. High Quality Monolayer Graphene Synthesized by Resistive Heating Cold Wall Chemical Vapor Deposition. *Adv. Mater.* **2015**, *27*, 4200–4206. [CrossRef] [PubMed]

13. Lee, H.C.; Jo, S.B.; Lee, E.; Yoo, M.S.; Kim, H.H.; Lee, S.K.; Lee, W.H.; Cho, K. Facet-Mediated Growth of High-Quality Monolayer Graphene on Arbitrarily Rough Copper Surfaces. *Adv. Mater.* **2016**, *28*, 2010–2014. [CrossRef] [PubMed]

14. Chen, X.; Xiang, R.; Zhao, P.; An, H.; Inoue, T.; Chiashi, S.; Maruyama, S. Chemical vapor deposition growth of large single-crystal bernal-stacked bilayer graphene from ethanol. *Carbon* **2016**, *107*, 852–856. [CrossRef]

15. Wu, J.; Wang, J.; Pan, D.; Li, Y.; Jiang, C.; Li, Y.; Jin, C.; Wang, K.; Song, F.; Wang, G.; et al. Synchronous Growth of High-Quality Bilayer Bernal Graphene: From Hexagonal Single-Crystal Domains to Wafer-Scale Homogeneous Films. *Adv. Funct. Mater.* **2017**, *27*, 1605927. [CrossRef]

16. Gibson, K.D.; Sibener, S.J. Growth, Structure, and Vibrational Properties of Few Layer Graphene Grown on Rh(111). *J. Phys. Chem. C* **2016**, *120*, 24158–24164. [CrossRef]

17. Soares, G.V.; Nakhaie, S.; Heilmann, M.; Riechert, H.; Lopes, J.M.J. Growth of boron-doped few-layer graphene by molecular beam epitaxy. *Appl. Phys. Lett.* **2018**, *112*, 163103. [CrossRef]

18. Weibel, A.; Mesguich, D.; Chevallier, G.; Flahaut, E.; Laurent, C. Fast and easy preparation of few-layered-graphene/magnesia powders for strong, hard and electrically conducting composites. *Carbon* **2018**, *136*, 270–279. [CrossRef]

19. Kairi, M.I.; Dayou, S.; Kairi, N.I.; Abu Bakar, S.; Vigolo, B.; Mohamed, A.R. Toward high production of graphene flakes—A review on recent developments in their synthesis methods and scalability. *J. Mater. Chem. A* **2018**, *6*, 15010–15026. [CrossRef]

20. Badri, M.A.S.; Salleh, M.M.; Noor, N.F.a.M.; Abd Rahman, M.Y.; Umar, A.A. Green synthesis of few-layered graphene from aqueous processed graphite exfoliation for graphene thin film preparation. *Mater. Chem. Phys.* **2017**, *193*, 212–219. [CrossRef]

21. Han, M.Y.; Oezyilmaz, B.; Zhang, Y.; Kim, P. Energy band-gap engineering of graphene nanoribbons. *Phys. Rev. Lett.* **2007**, *98*, 206805. [CrossRef] [PubMed]

22. Li, X.; Wang, X.; Zhang, L.; Lee, S.; Dai, H. Chemically derived, ultrasmooth graphene nanoribbon semiconductors. *Science* **2008**, *319*, 1229–1232. [CrossRef] [PubMed]

23. Luo, W.-G.; Wang, H.-F.; Cai, K.-M.; Han, W.-P.; Tan, P.-H.; Hu, P.-A.; Wang, K.-Y. Synthesis of Homogenous Bilayer Graphene on Industrial Cu Foil. *Chin. Phys. Lett.* **2014**, *31*, 067202. [CrossRef]

24. Pang, J.; Bachmatiuk, A.; Fu, L.; Yan, C.; Zeng, M.; Wang, J.; Trzebicka, B.; Gemming, T.; Eckert, J.; Rummeli, M.H. Oxidation as A Means to Remove Surface Contaminants on Cu Foil Prior to Graphene Growth by Chemical Vapor Deposition. *J. Phys. Chem. C* **2015**, *119*, 13363–13368. [CrossRef]

25. Xu, X.; Zhang, Z.; Dong, J.; Yi, D.; Niu, J.; Wu, M.; Lin, L.; Yin, R.; Li, M.; Zhou, J.; et al. Ultrafast epitaxial growth of metre-sized single-crystal graphene on industrial Cu foil. *Sci. Bull.* **2017**, *62*, 1074–1080. [CrossRef]

26. Wang, C.; Chen, W.; Han, C.; Wang, G.; Tang, B.; Tang, C.; Wang, Y.; Zou, W.; Chen, W.; Zhang, X.-A.; et al. Growth of Millimeter-Size Single Crystal Graphene on Cu Foils by Circumfluence Chemical Vapor Deposition. *Sci. Rep.* **2014**, *4*, 4537. [CrossRef] [PubMed]
27. Li, X.; Cai, W.; An, J.; Kim, S.; Nah, J.; Yang, D.; Piner, R.; Velamakanni, A.; Jung, I.; Tutuc, E.; et al. Large-Area Synthesis of High-Quality and Uniform Graphene Films on Copper Foils. *Science* **2009**, *324*, 1312–1314. [CrossRef] [PubMed]
28. Xin, H.; Li, W. A review on high throughput roll-to-roll manufacturing of chemical vapor deposition graphene. *Appl. Phys. Rev.* **2018**, *5*, 031105. [CrossRef]
29. Li, J.; Wang, X.-Y.; Liu, X.-R.; Jin, Z.; Wang, D.; Wan, L.-J. Facile growth of centimeter-sized single-crystal graphene on copper foil at atmospheric pressure. *J. Mater. Chem. C* **2015**, *3*, 3530–3535. [CrossRef]
30. Cai, S.; Liu, Z.; Zhong, N.; Liu, S.; Liu, X. Effect of Growth Pressure on Epitaxial Graphene Grown on 4H-SiC Substrates by Using Ethene Chemical Vapor Deposition. *Materials* **2015**, *8*, 5586–5596. [CrossRef] [PubMed]
31. Cai, T.; Jia, Z.; Yan, B.; Yu, D.; Wu, X. Hydrogen assisted growth of high quality epitaxial graphene on the C-face of 4H-SiC. *Appl. Phys. Lett.* **2015**, *106*, 013106. [CrossRef]
32. Hassan, J.; Winters, M.; Ivanov, I.G.; Habibpour, O.; Zirath, H.; Rorsman, N.; Janzen, E. Quasi-free-standing monolayer and bilayer graphene growth on homoepitaxial on-axis 4H-SiC(0001) layers. *Carbon* **2015**, *82*, 12–23. [CrossRef]
33. Liu, Q.; Yu, C.; He, Z.; Gu, G.; Wang, J.; Zhou, C.; Guo, J.; Gao, X.; Feng, Z. Chemical vapor deposition graphene of high mobility by gradient growth method on an 4H-SiC (0001) substrate. *Appl. Surf. Sci.* **2018**, *454*, 68–73. [CrossRef]
34. Liu, X.; Chen, Y.; Sun, C.; Guan, M.; Zhang, Y.; Zhang, F.; Sun, G.; Zeng, Y. Surface Evolution of Nano-Textured 4H-SiC Homoepitaxial Layers after High Temperature Treatments: Morphology Characterization and Graphene Growth. *Nanomaterials* **2015**, *5*, 1532–1543. [CrossRef] [PubMed]
35. Berger, C.; Song, Z.; Li, X.; Wu, X.; Brown, N.; Naud, C.; Mayou, D.; Li, T.; Hass, J.; Marchenkov, A.N.; et al. Electronic confinement and coherence in patterned epitaxial graphene. *Science* **2006**, *312*, 1191–1196. [CrossRef] [PubMed]
36. Cai, S.; Liu, X.; Huang, J.; Liu, Z. Feasibility of polyethylene film as both supporting material for transfer and target substrate for flexible strain sensor of CVD graphene grown on Cu foil. *RSC Adv.* **2017**, *7*, 48333–48340. [CrossRef]
37. Kim, W.; Kim, H.; Kim, G.T. Ultra-Easy and Fast Method for Transferring Graphene Grown on Metal Foil. *Nano* **2017**, *12*, 1750140. [CrossRef]
38. Camara, N.; Tiberj, A.; Jouault, B.; Caboni, A.; Jabakhanji, B.; Mestres, N.; Godignon, P.; Camassel, J. Current status of self-organized epitaxial graphene ribbons on the C face of 6H-SiC substrates. *J. Phys. D-Appl. Phys.* **2010**, *43*, 374011. [CrossRef]
39. Huang, Q.; Kim, J.J.; Ali, G.; Cho, S.O. Width-Tunable Graphene Nanoribbons on a SiC Substrate with a Controlled Step Height. *Adv. Mater.* **2013**, *25*, 1144–1148. [CrossRef] [PubMed]
40. Bishop, S.M.; Reynolds, C.L., Jr.; Liliental-Weber, Z.; Uprety, Y.; Ebert, C.W.; Stevie, F.A.; Park, J.S.; Davis, R.F. Sublimation growth of an in-situ-deposited layer in SiC chemical vapor deposition on 4H-SiC(1 1 (2)over-bar 0). *J. Cryst. Growth* **2008**, *311*, 72–78. [CrossRef]
41. Liu, B.; Sun, G.-S.; Liu, X.-F.; Zhang, F.; Dong, L.; Zheng, L.; Yan, G.-G.; Liu, S.-B.; Zhao, W.-S.; Wang, L.; et al. Fast Homoepitaxial Growth of 4H-SiC Films on 4 degrees off-Axis Substrates in a SiH4-C2H4-H-2 System. *Chin. Phys. Lett.* **2013**, *30*, 28101. [CrossRef]
42. Ishida, Y.; Yoshida, S. Investigation of the giant step bunching induced by the etching of 4H-SiC in Ar-H-2 mix gases. *Jpn. J. Appl. Phys.* **2016**, *55*, 095501. [CrossRef]
43. Kimoto, T.; Itoh, A.; Matsunami, H.; Okano, T. Step bunching mechanism in chemical vapor deposition of 6H- and 4H-SiC{0001}. *J. Appl. Phys.* **1997**, *81*, 3494–3500. [CrossRef]
44. Tabuchi, Y.; Ashida, K.; Sonoda, M.; Kaneko, T.; Ohtani, N.; Katsuno, M.; Sato, S.; Tsuge, H.; Fujimoto, T. Wide (0001) terrace formation due to step bunching on a vicinal 4H-SiC (0001) epitaxial layer surface. *J. Appl. Phys.* **2017**, *122*, 075702. [CrossRef]
45. Prakash, G.; Capano, M.A.; Bolen, M.L.; Zemlyanou, D.; Reifenberger, R.G. AFM study of ridges in few-layer epitaxial graphene grown on the carbon-face of 4H-SiC(000(1)over-bar). *Carbon* **2010**, *48*, 2383–2393. [CrossRef]

46. Ushio, S.; Yoshii, A.; Tamai, N.; Ohtani, N.; Kaneko, T. Wide-range temperature dependence of epitaxial graphene growth on 4H-SiC (0 0 0-1): A study of ridge structures formation dynamics associated with temperature. *J. Cryst. Growth* **2011**, *318*, 590–594. [CrossRef]

47. Bouhafs, C.; Darakchieva, V.; Persson, I.L.; Tiberj, A.; Persson, P.O.A.; Paillet, M.; Zahab, A.A.; Landois, P.; Juillaguet, S.; Schoeche, S.; et al. Structural properties and dielectric function of graphene grown by high-temperature sublimation on 4H-SiC(000-1). *J. Appl. Phys.* **2015**, *117*, 085701. [CrossRef]

48. Krzyzewski, F. 4H-SiC surface structure transitions during crystal growth following bunching in a fast sublimation process. *J. Cryst. Growth* **2014**, *401*, 511–513. [CrossRef]

49. Ferrari, A.C.; Meyer, J.C.; Scardaci, V.; Casiraghi, C.; Lazzeri, M.; Mauri, F.; Piscanec, S.; Jiang, D.; Novoselov, K.S.; Roth, S.; et al. Raman spectrum of graphene and graphene layers. *Phys. Rev. Lett.* **2006**, *97*, 187401. [CrossRef] [PubMed]

50. Martins Ferreira, E.H.; Moutinho, M.V.O.; Stavale, F.; Lucchese, M.M.; Capaz, R.B.; Achete, C.A.; Jorio, A. Evolution of the Raman spectra from single-, few-, and many-layer graphene with increasing disorder. *Phys. Rev. B* **2010**, *82*, 125429. [CrossRef]

51. Thomsen, C.; Reich, S. Doable resonant Raman scattering in graphite. *Phys. Rev. Lett.* **2000**, *85*, 5214–5217. [CrossRef] [PubMed]

52. Strudwick, A.J.; Creeth, G.L.; Johansson, N.A.B.; Marrows, C.H. Probing residual strain in epitaxial graphene layers on 4H-SiC (000(1)over-bar) with Raman spectroscopy. *Appl. Phys. Lett.* **2011**, *98*, 051910. [CrossRef]

53. Rana, T.; Chandrashekhar, M.V.S.; Sudarshan, T.S. Vapor phase surface preparation (etching) of 4H-SiC substrates using tetrafluorosilane (SiF4) in a hydrogen ambient for SiC epitaxy. *J. Cryst. Growth* **2013**, *380*, 61–67. [CrossRef]

54. Dong, L.; Sun, G.; Yu, J.; Zheng, L.; Liu, X.; Zhang, F.; Yan, G.; Li, X.; Wang, Z. Growth of 4H-SiC epilayers with low surface roughness and morphological defects density on 4 degrees off-axis substrates. *Appl. Surf. Sci.* **2013**, *270*, 301–306. [CrossRef]